Ferromagnetic and incommensurate antiferromagnetic order in a multi-sublattice itinerant magnet: $Y_3Co_8Sn_4$

2005 J. Phys.: Condens. Matter 17 373

(http://iopscience.iop.org/0953-8984/17/2/012)

INSTITUTE OF PHYSICS PUBLISHING JOURNAL OF PHYSICS: CONDENSED MATTER

J. Phys.: Condens. Matter **17** (2005) 373–383 doi:10.1088/0953-8984/17/2/012

Ferromagnetic and incommensurate antiferromagnetic order in a multi-sublattice itinerant magnet: $Y_3Co_8Sn_4$

F Canepa[1], M Napoletano[1], A Palenzona[1], O Moze[2] and W Kockelmann[3]

[1] INFM, Dipartimento di Chimica e Chimica Industriale, Università degli Studi di Genova, Via Dodecaneso 31, 16146, Genova, Italy
[2] INFM, Dipartimento di Fisica, Università degli Studi di Modena e Reggio Emilia, Via G Campi 213/a, 41100 Modena, Italy
[3] ISIS Facility, Rutherford Appleton Laboratory, Chilton, Didcot OX11 OQX, UK

E-mail: moze@unimore.it

Received 26 October 2004, in final form 7 December 2004
Published 20 December 2004
Online at stacks.iop.org/JPhysCM/17/373

Abstract

Neutron diffraction, ac susceptibility and low field dc magnetic measurements were performed on the ternary intermetallic phase $Y_3Co_8Sn_4$. This compound displays a ferromagnetic transition at 53 K and then undergoes a further transition below 10 K into an incommensurate antiferromagnetic modulated structure. The low temperature magnetic structure is a long period sine or helical modulation with a propagation vector of [0.095, 0, 0] corresponding to a modulation length of about 80 Å at 1.6 K. A possible mechanism for such a peculiar behaviour is a change from a high temperature itinerant character of the magnetic interactions to a low temperature localized magnetic state in a multi-sublattice system.

1. Introduction

The series of intermetallic compounds $R_3Co_8Sn_4$ (R from Pr to Lu and Y) has been recently synthesized and their crystallographic structure [1] and magnetic properties [2–5] have been widely investigated. They crystallize in the $Lu_3Co_{7.77}Sn_4$ structure type (space group $P6_3mc$) with a full occupancy of atomic positions and display ferro- or ferri-magnetic behaviour with respect to the type of R atom considered. The compounds with R = Pr and Nd also display a spin reorientation transition at low temperatures. Of particular interest is the intriguing behaviour of the zero-field cooled and field cooled thermomagnetic curves and of the in-phase χ' and out-of-phase χ'' components of the ac susceptibility, which has been detected in $Tb_3Co_8Sn_4$ [4] and $Dy_3Co_8Sn_4$ [5] compounds and tentatively ascribed to either a re-entrant spin glass state or movement of domain walls.

The magnetic properties of the Co sublattices in $Y_3Co_8Sn_4$ have been previously reported [1]. The thermal dependence of the magnetization in fields of up to 9 T implies that ferromagnetic order sets in below 62 K, with a low saturation Co moment of 0.3 μ_B at 5 K and 9 T. The itinerant nature of the Co sublattices has been confirmed via the observed linear dependence of the spontaneous magnetization squared, $M_s^2(T)$ versus T^2 (T = temperature) [6]. As the crystal structure presents one (R) rare earth and four different Co sublattices, the multi-sublattice nature of Co magnetic moments may induce competing exchange interactions between these sites, giving rise to an unexpectedly complex and peculiar behaviour of the magnetic structure of this system. A recent neutron diffraction investigation of $Y_3Co_8Sn_4$ has shown no indication of either ferromagnetic order or antiferromagnetic order down to 1.5 K [7]. In this work, it was reported that the Co magnetic contribution to the neutron diffraction patterns was not visible owing to a very low Co magnetic moment, for which electronic band structure calculations (TB-LMTO) give an upper limit of 0.10 μ_B. We report in this paper new details of the magnetic structure for $Y_3Co_8Sn_4$ and in particular the temperature dependence of the magnetic structure as studied and modelled by time-of-flight neutron powder diffraction and the linear and non-linear components of the ac susceptibility. These measurements furthermore provide clear evidence for the presence of long range magnetic ordering in this compound.

2. Experimental details

Samples of $Y_3Co_8Sn_4$ were prepared from 99.9 wt% pure Y and Co, and 99.999 wt% Sn by melting stoichiometric amounts of these elements in an induction furnace followed by annealing in silica tubes at 1073 K for 4 weeks under vacuum. Weight losses during the sample preparation were always below 1%. The ac susceptibility measurements were performed on an Oxford Maglab^{2000} platform operating in the temperature range 3–100 K. Linear and nonlinear susceptibilities are defined from the expansion of the magnetization M with respect to the applied field H [8]:

$$M = \chi_0 H + \chi_1 H^2 + \chi_2 H^3 + \cdots \tag{1}$$

where χ_0 is the linear susceptibility and χ_1 and χ_2 are non-linear terms. In the demagnetized state, the magnetization M has inversion symmetry with respect to the applied magnetic field [9, 10], so that $\chi_1 = \chi_3 \cdots = 0$. The linear and non-linear susceptibilities were detected by a lock-in system (Stanford RS830) using the fundamental and the third order harmonics. In the present investigation we present the in-phase (χ') and the out-of-phase (χ'') parts of the linear susceptibility and the magnitude of the in-phase component of the third order susceptibility (χ_2').

The neutron powder diffraction experiments were carried out on the time-of-flight diffractometer ROTAX located at the pulsed neutron source ISIS, Rutherford Appleton Laboratory, UK. The powdered sample of $Y_3Co_8Sn_4$ was filled under He exchange gas into a thin-walled cylindrical vanadium container of 6 mm diameter, which was mounted into the sample chamber of a closed-cycle refrigerator. The sample cell, equipped with vanadium windows for the primary neutron beam to pass through, was filled with He exchange gas to ensure good thermal contact between sample container and cold plate. Data were collected at 293 K and at temperatures between 70 and 10 K. Additional neutron diffraction data were recorded at 1.6 and 30 K, with the sample material inserted into a 6 mm aluminium container and installed in an LHe flow cryostat equipped with aluminium windows, thus minimizing instrument background with respect to incoherent scattering, at the cost of introducing aluminium Bragg peaks into the diffraction patterns. For both set-ups data were collected

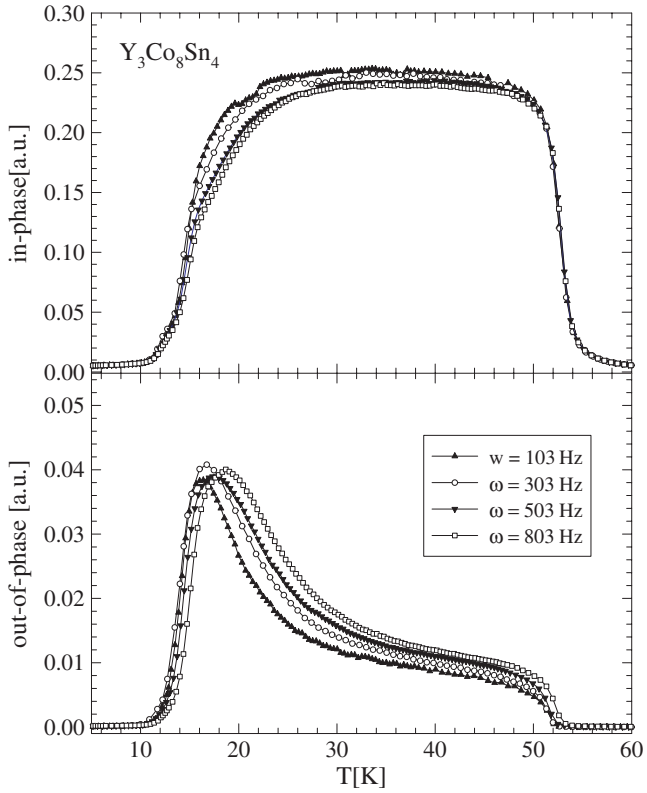

Figure 1. The frequency dependence of the in-phase and out-of-phase components of the ac susceptibility for $Y_3Co_8Sn_4$ between 5 and 70 K ($\mu_0 H_{ac} = 1$ mT).

using three fixed-angle position-sensitive detectors at 2θ scattering angles of 17.2° (bank 1), 52.6° (bank 2) and 122.2° (bank 3).

3. Analysis and results

Previous dc magnetic measurements performed on $Y_3Co_8Sn_4$ suggested a ferromagnetic transition at 62 K [2]: the transition temperature obtained from an Arrott plot is consistent with an inflection point at around 60 K observed in the magnetization isotherm measured in a field of 1 T. At 5 K the saturation value of the magnetic moment, in a field of 9 T, is 0.32 μ_B/Co atom.

3.1. Ac susceptibility

Figure 1 shows the dependence of χ' and χ'' at selected frequencies. The real part χ' increases sharply at 53 K where ferromagnetic order sets in, and then remains almost constant between 20 and 50 K. It then decreases towards very low values with a path which is frequency dependent. A change of slope is observed around 15 K. The frequency dependence is more evident in χ'': a broad peak (corresponding to the inflection point in χ') is observed between 15 and 20 K and the maximum shifts towards higher temperatures with increasing frequency. In contrast, an S-shaped behaviour, which is slightly frequency dependent, reveals the ferromagnetic transition at 53 K. In figure 2, the in-phase component of the third order susceptibility is reported. The

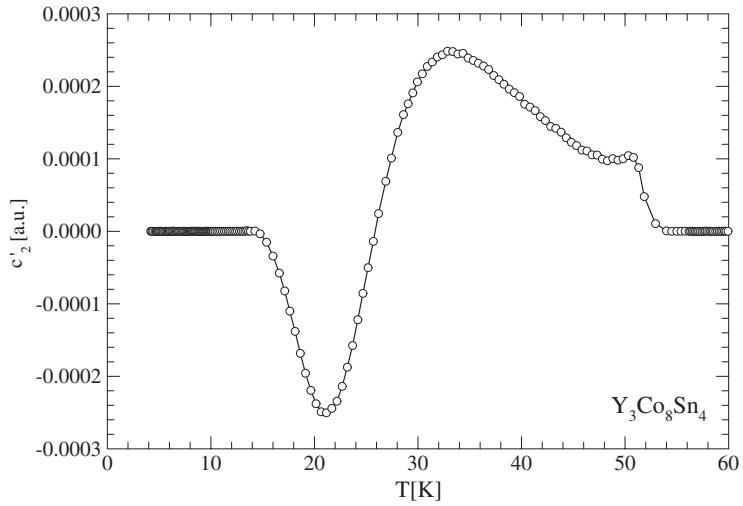

Figure 2. The in-phase component of the third order susceptibility, χ_2', for $Y_3Co_8Sn_4$ between 5 and 70 K.

ferromagnetic transition is clearly observed at 53 K, whilst a negative peak is visible at around 21 K. The difference observed in the Curie temperature values, 53 versus 62 K, obtained from different measurements is related to the method used: the measure of T_c from ac susceptibility data is very accurate because it is a direct method and the magnetic ac field displays only a perturbing action on the magnetic structure, while the evaluation of T_c from the inflexion point in the thermal dependence of the magnetization or from the Arrott plot is generally considered a rough estimate [11, 12].

3.2. Dc magnetization

The low field dependence of the magnetization at selected temperatures is reported in figure 3: at 3 K a linear increase of the magnetization is followed by a field induced transition at a threshold field of 48 mT. With increasing temperatures the threshold field decreases and vanishes above 10 K and is not observed in the curve at 30 K, where a typical ferromagnetic behaviour is detected. The zero-field cooled (ZFC) and field cooled (FC) magnetization curves, in an applied field of 20 mT, are practically identical: in both curves very low values between 4 and 10 K are observed, followed by a sharp increase of the magnetization up to 20 K. At higher temperatures the magnetization decreases again, displaying a change of slope corresponding to the ferromagnetic transition.

3.3. Neutron diffraction

Rietveld profile analysis of the neutron diffraction data was performed with the GSAS suite of programs [13] by a three-bank refinement of crystal and magnetic structure parameters. The neutron scattering lengths used were $b_Y = 7.75$ fm, $b_{Co} = 2.53$ fm and $b_{Sn} = 6.23$ fm. Absorption caused by the sample, the sample container and the cryostat windows was accounted for by fitting a parameter for linear absorption with one common parameter for the three diffractometer histograms. The time-of-flight peak shapes were accounted for by fitting parameters of a 'double-exponential pseudo-Voigt' function provided by GSAS. Refinement

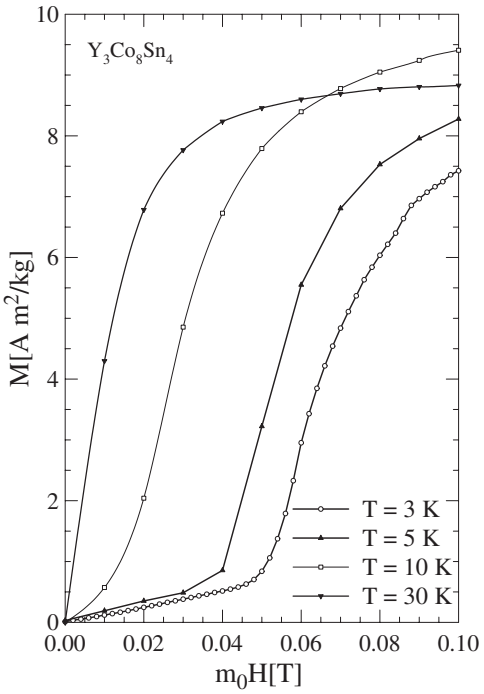

Figure 3. Low field magnetization curves for $Y_3Co_8Sn_4$.

Table 1. Refined crystal structure parameters $Y_3Co_8Sn_4$ at 30 K. Isotropic displacement parameters are refined for each atom type. Selected shortest interatomic distances between Co atoms are also displayed.

Atom	Site	x	y	z	u_{iso} (Å^2)
Y	6c	0.5277(1)	0.4723(1)	0.000 000	0.0040(4)
Co_1	6c	0.1618(3)	0.8382(3)	0.1629(4)	0.0045(4)
Co_2	6c	0.0986(2)	0.9014(2)	0.4751(5)	0.0045(4)
Co_3	2b	1/3	2/3	0.8137(8)	0.0045(4)
Co_4	2a	0.0	0.0	0.7222(8)	0.0045(4)
Sn	6c	0.1704(1)	0.8297(1)	0.7933(3)	0.0034(2)
Sn	2b	1/3	2/3	0.1795(3)	0.0034(2)
Co_1–Co_1	4.299(7) Å		Co_2–Co_2	2.621(5) Å	
Co_1–Co_2	2.522(5) Å		Co_2–Co_3	4.398(5) Å	
Co_1–Co_3	3.703(6) Å		Co_2–Co_4	2.385(6) Å	
Co_1–Co_4	2.521(4) Å		Co_4–Co_4	3.729(5) Å	

of the room temperature data clearly showed that the sample is single phase. The refined lattice parameters from the room temperature neutron powder data are $a = 8.8784(1)$ Å and $c = 7.4860(2)$ Å. The low temperature lattice parameters are $a = 8.8566(1)$ Å, $c = 7.4584(1)$ Å and $a = 8.8568(1)$ Å, $c = 7.4575(1)$ Å at 30 and 10 K, respectively. The crystal space group is $P6_3mc$ with Y occupying the 6c site $(x, -x, z)$; Co atoms occupy two in-equivalent 6c sites as well as 2b $(1/3, 2/3, z)$ and 2a $(0, 0, z)$ sites. The Sn atoms occupy two sites, 6c and 2b. The refined crystal structure parameters $Y_3Co_8Sn_4$, compiled in table 1 for 30 K, are consistent with the results from single-crystal and powder x-ray studies [1]. Table 1

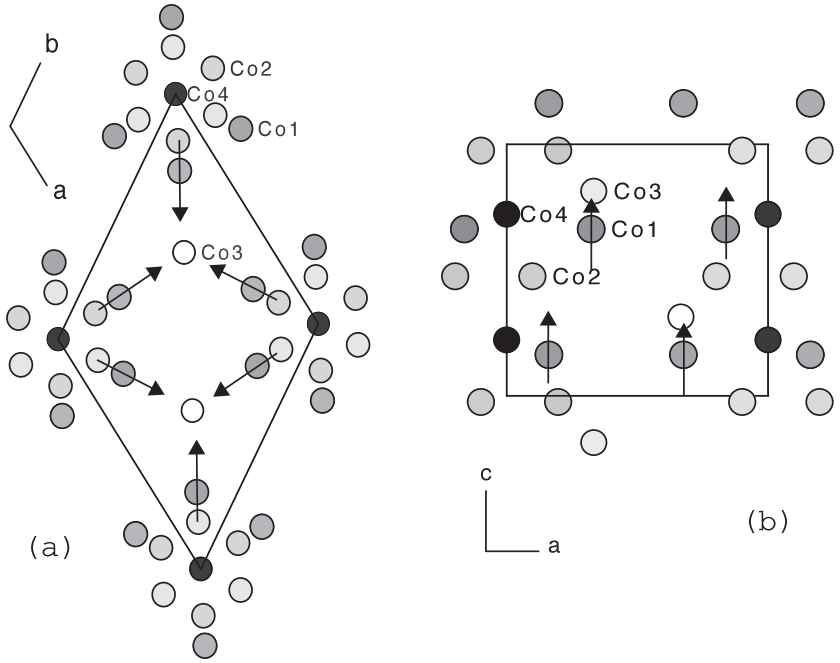

Figure 4. Co sublattices in $Y_3Co_8Sn_4$ (Co1, dark shaded; Co2, light shaded; Co3, white; Co4, black). Y and Sn atoms are omitted for reasons of simplicity. Arrows indicate magnetic moment directions for $P6_3m'c'$, only for Co1 atoms for reasons of clarity. (a) Projection along ⟨001⟩ and antiferromagnetic basal plane magnetic moments. (b) Projection along ⟨010⟩ and ferromagnetic alignment of Co1 moments along the *c*-axis.

also contains selected interatomic distances of Co atoms in $Y_3Co_8Sn_4$. As reported previously in the x-ray study, all Co atoms, apart from the 2b site, have a coordination number of 12, and reside in a more or less distorted icosahedral environment. Figure 4 shows projections of the crystal structure along ⟨001⟩ and ⟨010⟩ directions, displaying the Co sites only. The coordination number of Co at the 2b site is 10 and this site, significantly, has no Co nearest neighbours. Profile fitted neutron diffraction patterns collected at 30 and 10 K are displayed in figure 5.

For temperatures below 50 K, a weak (100) peak of magnetic origin appears at a *d*-spacing of 7.67 Å (figure 5), whereas magnetic peaks such as (001) at 7.46 Å, (101) at 5.35 Å and (110) at 4.43 Å are conspicuous by their absence. The (001) reflection has zero intensity for ferromagnetic and antiferromagnetic sublattice configurations. Model calculations show that (101) and (110) magnetic intensities are much weaker than the (100) intensity for the relevant magnetic structure models. This is why magnetic Bragg intensity is clearly only observed at the (100) peak position at 30 K. The temperature dependence of the integrated peak intensity at the (100) position is displayed in figure 6. On further cooling down to 10 K the magnetic (100) reflection disappears whereas small peaks appear in the vicinity of the (100) position. The splitting of the magnetic (100) into four weak magnetic satellite peaks below 10 K is evident from the difference pattern between 30 and 1.6 K (figure 7). We therefore identify two magnetic phases, a commensurate magnetic phase between 10 and 53 K (magnetic phase 1) and an incommensurate magnetic phase at 10 K and below (magnetic phase 2).

Due to the small magnitude of the expected Co moment and to the significant neutron absorption cross-section of Co, the intensities of magnetic peaks are expected to be very small

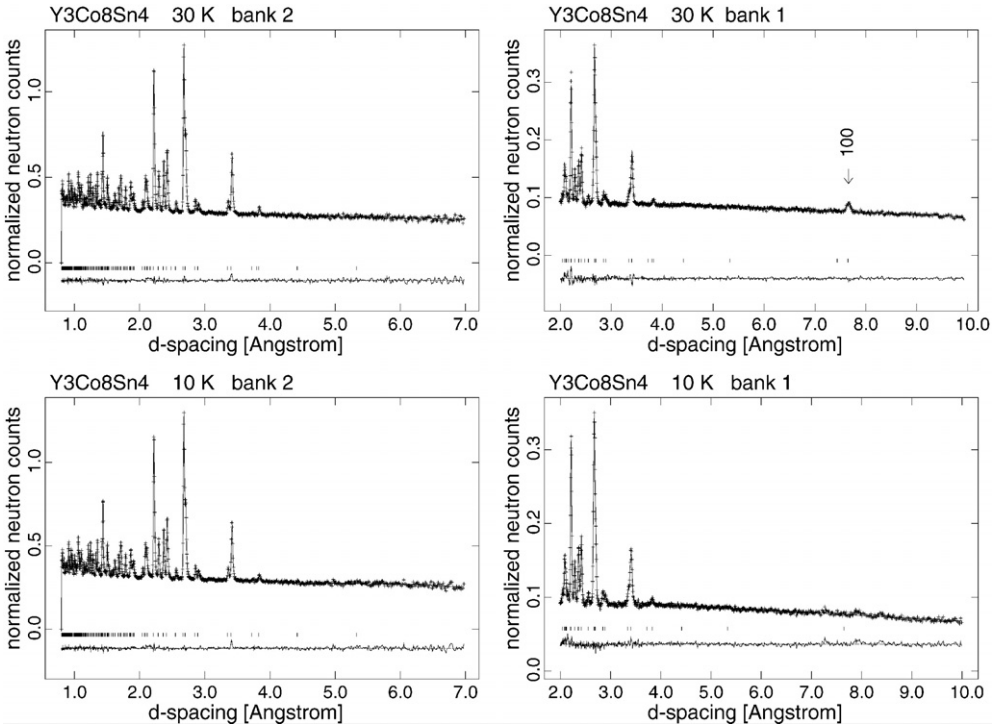

Figure 5. Observed and calculated neutron diffraction pattern of $Y_3Co_8Sn_4$ at 30 K (above) and at 10 K (below) displaying detector bank 1 (right) and bank 2 (left). The (100) magnetic peak at 30 K is marked at a *d*-spacing of 7.67 Å.

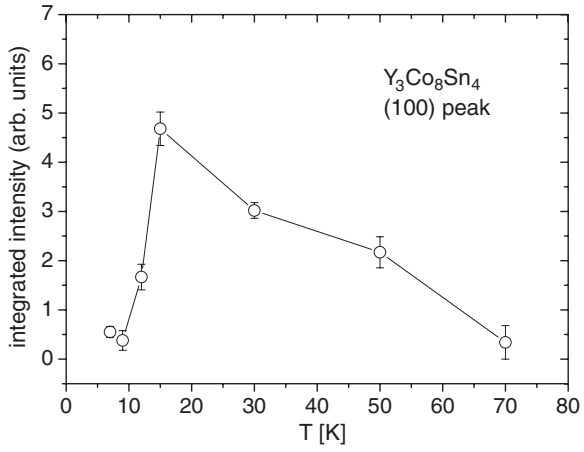

Figure 6. Temperature dependence of the (100) integrated intensity of $Y_3Co_8Sn_4$ between 70 and 10 K. The small intensity at 70 K for the (100) peak reflects the uncertainties due to poor statistics; there is no (100) peak discernible in the diffraction pattern.

with respect to the nuclear intensities. In fact, only one and four weak peaks are discernible above and below 10 K, respectively. Magnetic satellites observed below 10 K are barely noticeable above the neutron incoherent background. For the set-up of a magnetic structure

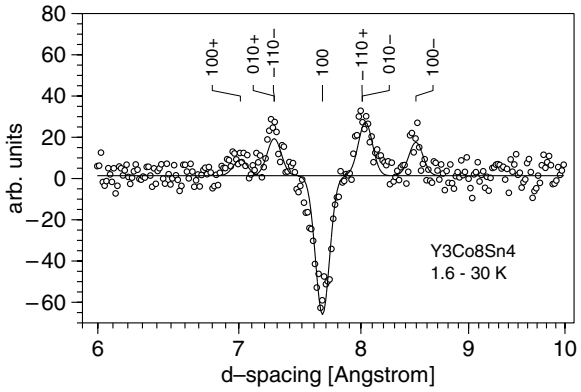

Figure 7. Difference between 1.6 and 30 K patterns (circles) for $Y_3Co_8Sn_4$. The solid curve represents calculated peak profiles of the commensurate ferromagnetic structure (negative peak at 7.67 Å) and an incommensurate sinusoidal modulation (positive peaks). Labels '$(hkl)\pm$' of the satellite reflections stand for $(h, k, l) \pm \mathbf{k}_2$.

model, it was therefore necessary to keep the number of magnetic structure parameters to a minimum. Observation of a (100) magnetic peak above 10 K and absence of a (001) peak confirm preservation of the reflection condition imposed by the 6_3 screw axis of the crystal space group $P6_3mc$. As (100) corresponds to a reciprocal lattice point of the crystal lattice the magnetic propagation vector for the phase between 10 and 53 K is assumed to be $k_1 = [0, 0, 0]$. This modulation vector may include ferromagnetic, ferrimagnetic and antiferromagnetic configurations of the four magnetic Co sublattices. In accordance with the results of the magnetic susceptibility measurements we only consider models consistent with the ferromagnetic space group $P6_3m'c'$ for $P6_3mc$ [14, 15] in order to retain a high magnetic symmetry. The admissible magnetic site symmetries of the Co atoms are m' (site 6c) and $3m'$ (sites 2b, 2a). The magnetic anti-mirror vertical plane m' allows moment directions parallel to the m' mirror plane. These directions can be in the hexagonal basal plane and along the c-axis as well as intermediate moment directions inclined to the c-axis. We discuss here only magnetic moments parallel (axial model) and perpendicular (planar models) to the c-axis. The two models are illustrated in figure 4 for the Co_1 site. Whereas magnetic site symmetry m' of Co_1 and Co_2 allows for axial and planar models, $3m'$ of Co_3 and Co_4 on sites 2b and 2a restrict the magnetic moments parallel to the c-axis. The planar model involves antiferromagnetic arrangements of moments whereas the axial model represents ferromagnetic alignment of Co moments in the respective Co sublattices. Admissible magnetic moment components are given in table 2. Parallel and antiparallel orientations of ferromagnetically ordered Co sublattices lead to ferro- and ferrimagnetic structures, respectively.

For the analysis of the neutron data in the temperature range 10–50 K based within the magnetic space group $P6_3m'c'$, Co moments on different sites were constrained in the refinements to have the same moment magnitudes in order to further reduce the number of variable parameters. For both the axial and the planar models there is only the size of the magnetic Co moment to be refined along with the crystal structure parameters (table 1). Due the large d-spacing range from 0.3 to 20 Å covered by the detector banks in the time-of-flight set-up, the correlation of the magnetic moment magnitude with absorption and atomic displacement parameters is minimized. In refinements of the magnetic moment, the magnetic form factor for Co, calculated for a spherical $\langle j_0 \rangle$ form factor expansion as implemented in the GSAS program, was used [16]. Table 2 contains the refined moments for axial and planar

Table 2. Refined magnetic structure parameters of $Y_3Co_8Sn_4$ at 30 K with $k_1 = [0, 0, 0]$. Components m_x, m_y, m_z refer to moment values along the crystal axes. R_{wp} denotes the Rietveld weighted profile R value for bank 1.

Site	Magnetic site symmetry	Axial m_z (μ_B)	Planar $m_x = -m_y$ (μ_B)
Co_1 (6c)	m'	0.34(2)	0.38(2)
Co_2 (6c)	m'	0.34	0.38
Co_3 (2b)	$3m'$	0.34	0
Co_4 (2a)	$3m'$	0.34	0
Moment/Co atom (μ_B)		0.34(2)	0.54(3)
Moment/unit cell (μ_B)		5.4	6.5
R_{wp} (%)		2.5	2.6

models, whilst the corresponding fits of the axial model are displayed in figure 5 for the low angle banks at 30 K.

For both the axial and planar models, the (100) reflection is the dominant peak. The same is true for ferro- and ferrimagnetic couplings of magnetic sublattices. In fact, for the $Y_3Co_8Sn_4$ configuration the magnetic (100) intensity is proportional to the square of the sublattice magnetic moment, and less sensitive to the mutual parallel or antiparallel alignment of sublattices. This means that ferro- and ferrimagnetic models are practically indistinguishable from the present diffraction data, with the refined moment magnitudes varying by 10%. Even though the Rietveld fit quality R factors are almost identical, the axial model is favoured from a symmetry point of view as it permits ordered magnetic moments on all four sites. More importantly, the axial ferromagnetic model is supported by the bulk susceptibility data. We therefore conclude that the magnetic structure in the temperature range 10–53 K is ferromagnetic with magnetic moments aligned along the c-axis. The moment magnitude for this preferred model is 0.34 μ_B/Co atom. This value is in excellent accord with the moment value determined from the bulk magnetization and susceptibility data (0.32 μ_B/Co atom at 5 K). In this context, with reference to table 2, it can be seen that the planar model also yields a much higher magnetic moment per Co atom (0.54 μ_B).

On cooling down to 10 K the structure transforms from a ferromagnet into a modulated antiferromagnetic configuration. This is indicated by the disappearance of the ferromagnetic (100) peak (figure 6), or more precisely, the splitting of the (100) peak into four weak magnetic satellite reflections (figure 7) around the (100) peak position. The satellites can be indexed with a magnetic propagation vector $k_2 = [k_x, 0, 0]$ with $k_x \sim 0.1$. The fundamental (100) reflection has a multiplicity of 6, (100), (010), (110) plus those related by inversion symmetry. A wavevector $[k_x, 0, 0]$ generates six satellites, one pair for each fundamental point, if higher order reflections are neglected. The (010) and $(\bar{1}10)$ satellites coincide, leaving a total of four distinguishable magnetic satellites for (100) in a powder diffraction pattern. Analysis of the positions of the four satellite reflections at 10 K and a least-squares refinement of the propagation vector leads to $k_2 = [0.092(2), 0, 0]$. At 1.6 K the propagation vector changes only slightly to $k_2 = [0.095(2), 0, 0]$, corresponding to a modulation periodicity of about 80 Å. It should be noted that symmetry equivalent propagation vectors $[0, k_x, 0]$ and $[-k_x, k_x, 0]$ generate the same magnetic diffraction pattern. In a similar vein to the commensurate phase described above, the present neutron data do not allow us to unambiguously determine the spin structure. The magnetic Co moment configuration can be regarded as a long period helical modulation or sine modulation of the fundamental magnetic structure. Since we cannot exclude a spin reorientation from axial to a planar moment arrangement across the

commensurate–incommensurate transition at 10 K, a helical modulation of a basic antiferromagnetic structure as sketched for the Co_1 lattice in figure 4 cannot be excluded. On the other hand, if no reorientation of moments takes place across the transition at 10 K, the low temperature magnetic structure can be regarded as long period modulation of the high-temperature ferromagnetic structure. In this case the compound is an incommensurate antiferromagnet with a predominant ferromagnetic coupling between neighbouring Co atoms.

The observation of a small ferromagnetic moment of 0.34 μ_B, and the ensuing splitting of the ferromagnetic Bragg intensity into satellites, is at the limit of detection for neutron powder diffraction experiments. Therefore, the analysis of the incommensurate magnetic structure has to remain at a semi-quantitative level. By considering the axial ferromagnetic structure as the most likely one the structure below 10 K is assumed to be sinusoidal. Figure 7 shows the difference diffraction pattern between 1.6 and 30 K and indicates that the integrated intensity of the ferromagnetic (100) peak and the sum of the satellite intensities are approximately the same. The peak profiles were calculated with the program POWLS [17] by assuming that the ordered moment per Co atom in the ferromagnetic phase is preserved in the modulated antiferromagnetic phase. A sinusoidal structure with Co moments parallel to the *c*-axis and a sine wave amplitude of 0.48 μ_B that corresponds to an average moment value of 0.34 μ_B at 30 K yields a reasonable agreement between observed and calculated intensities. A square-modulated, equal-moment structure with moments of 0.34 μ_B would also produce the same satellite pattern, assuming that higher order reflections are too small to be observed in the present powder diffraction investigation. Our results contrast earlier neutron diffraction measurements which did not evidence any magnetic order down to 1.5 K [7].

4. Discussion and conclusions

In the $Lu_3Co_{7.77}Sn_4$ structure, Co atoms located on the 2b site have no other Co atoms as nearest neighbours. This supports the hypothesis of a localization of the d electrons of the Co atoms at that site. As far as the other Co atoms are concerned, some of the Co–Co distances are close to or well below the sum of the Co atomic radii ($r_{Co} = 1.25$ Å), leading to the formation of a band responsible for the magnetic properties. Previously obtained magnetic data for $Y_3Co_8Sn_4$ indicated a simple ferromagnetic order below 62 K, but rather surprisingly the present ac susceptibility measurements display a clear frequency dependent transition around 20 K. The susceptibility maxima are shifted towards higher temperatures with increasing frequency. This is generally considered a typical feature of a spin glass or spin-glass-like transition. According to the phenomenological theory of Suzuki [18], in a spin glass system there should be a negative divergence in the second derivative of the non-linear susceptibility with respect to the temperature. Indeed, we observe a negative peak (but not a divergence) in χ_2'. Moreover the crystal structure with isolated Co atoms could in some way provide frustrated competing magnetic interactions between the Co atoms which is a prerequisite for the existence of a spin glass state. Following this hypothesis further ac susceptibility measurements with a constant acquisition frequency and an increasing bias dc field were performed. The peak related to the hypothetical spin glass transition was clearly inhibited and shifted towards lower temperatures with increasing bias dc field, in contrast with a typical spin glass behaviour which is generally unaffected by a superimposed magnetic field. The dc magnetization curves measured in the ZFC and FC states are not consistent with a spin glass behaviour: rather than diverging at a spin glass transition temperature, no difference between the ZFC and FC curves could be observed for $Y_3Co_8Sn_4$ and both display a ZFC behaviour. Below 10 K, the magnetization displays a linear increase with rising magnetic field followed by a field induced transition: this behaviour strongly indicates an antiferromagnetic ground state, instead of a spin glass state, which is

suppressed when the temperature is increased above 20 K. This new hypothesis is consistent with the shift towards a lower temperature of the 20 K transition in the ac susceptibility with increasing bias dc field and with the observed ZFC and FC behaviour.

The neutron diffraction data confirm this unusual and most peculiar behaviour of the magnetic structure. The structure in zero field changes from that of a high temperature ferromagnet to a low temperature incommensurate antiferromagnet. The structure can be regarded as a modulated ferromagnet for which a ferromagnetic coupling remains on cooling below 10 K but the moment arrangement is subjected to a long range modulation. The frequency dependence of the ac susceptibility and the peak observed in the third harmonic could result from a frustration of short range ferromagnetic interactions in a long range antiferromagnetic ordered state. Furthermore, the observed ferromagnetic–antiferromagnetic transition implies a change from an itinerant character of the high temperature ferromagnetic phase to a more localized state of the low temperature antiferromagnetic state.

Acknowledgments

The authors wish to thank the INFM (Istituto Nazionale per la Fisica della Materia) for financial support. One of the authors (O Moze) is also grateful to the Consiglio Nazionale delle Ricerche for financial support.

References

[1] Canepa F, Cirafici S, Fornasini M L, Manfrinetti P, Merlo F, Palenzona A and Pani M 2000 *J. Alloys Compounds* **297** 109
[2] Canepa F, Napoletano M, Manfrinetti P, Palenzona A, Cirafici S and Merlo F 2000 *J. Magn. Magn. Mater.* **220** 39
[3] Canepa F, Napoletano M, Manfrinetti P and Cirafici S 2001 *J. Alloys Compounds* **314** 29
[4] Canepa F, Manfrinetti P, Napoletano M and Cirafici S 2001 *J. Alloys Compounds* **317/318** 556
[5] Canepa F and Napoletano M 2001 *J. Alloys Compounds* **325** L4
[6] Wohlfarth E P 1968 *J. Appl. Phys.* **39** 1061
[7] Gondek L, Szytula A, Baran S, Szajek A and Hernandez-Velasco J 2004 *Physica* B **350** E123
[8] Sato T and Miyako Y 1981 *J. Phys. Soc. Japan* **51** 1394
[9] Chakravarti A, Ranganathan R and Chatterjee S 1994 *J. Magn. Magn. Mater.* **138** 329
[10] Bitoh T, Ohba K, Takamatsu M, Shirane T and Chikazawa S 1996 *J. Magn. Magn. Mater.* **15** 59
[11] Crangle J C 1977 *The Magnetic Properties of Solids* (London: Edward Arnold)
[12] Takahashi M T 1991 *Physics and Engineering Applications of Magnetism* ed Y Ishikawa and N Miura (Berlin: Springer) chapter 7
[13] Larson A C and Von Dreele R B 1994 General structure analysis system (GSAS) *Los Alamos National Laboratory Report* LAUR 86-748
[14] Opechowski W and Guccione R 1963 *Magnetic Symmetry in Magnetism* vol IIA, ed G T Rado and H Suhl (New York: Academic) p 105
[15] Marshall W and Lovesey S W 1971 *Theory of Thermal Neutron Scattering* (Oxford: Oxford University Press) chapter 7
[16] Brown P J 1995 Magnetic form factors *International Tables for Crystallography* vol C, ed A J C Wilson (Dordrecht: Kluwer–Academic) p 391
[17] Kockelmann W 1995 *Berichte des Forschungszentrum Jülich,* Jül-3025, ISSN 0944-2952
[18] Suzuki M 1977 *Prog. Theor. Phys.* **58** 1151